



# Manganese(II) complexes of 2,3,5,6-tetra-(2-pyridyl)pyrazine – Syntheses, crystal structures, spectroscopic, magnetic and catalytic properties

B. Machura<sup>a,\*</sup>, J. Palion<sup>a</sup>, J. Mroziński<sup>b</sup>, B. Kalińska<sup>b</sup>, M. Amini<sup>c</sup>, M.M. Najafpour<sup>d</sup>, R. Kruszynski<sup>e</sup>

<sup>a</sup> Department of Crystallography, Institute of Chemistry, University of Silesia, 9th Szkolna St., 40-006 Katowice, Poland

<sup>b</sup> Faculty of Chemistry, Wrocław University, F. Joliot-Curie 14 St., 50-383 Wrocław, Poland

<sup>c</sup> Department of Chemistry, Faculty of Science, University of Maragheh, Golshahr, P.O. Box 55181-83111731, Maragheh, Iran

<sup>d</sup> Department of Chemistry, Institute for Advanced Studies in Basic Sciences, 45195-1159 Gava Zang, Zanjan, Iran

<sup>e</sup> Department of X-ray Crystallography and Crystal Chemistry, Institute of General and Ecological Chemistry, Technical University of Lodz, 116 Żeromski St., 90-924 Łódź, Poland

## ARTICLE INFO

### Article history:

Received 14 September 2012

Accepted 8 January 2013

Available online 29 January 2013

### Keywords:

Manganese(II)

2,3,5,6-Tetra-(2-pyridyl)pyrazine

X-ray structure

Magnetic properties

Catalytic activity

## ABSTRACT

A systematic studies on complex formation between Mn(II) ions, 2,3,5,6-tetra(2-pyridyl)pyrazine and halide or pseudohalide ( $N_3^-$ ,  $NCS^-$  and  $N(CN)_2^-$ ) ligands have been carried out and the following complexes  $[Mn_2(\mu-Cl)_2Cl_2(tppz)_2]$  (**1**),  $[Mn_2Cl_2(\mu-N_3-\kappa N1)_2(tppz)_2]$  (**2**),  $[MnCl(SCN)(tppz)(H_2O)] \cdot H_2O$  (**3**),  $[MnCl(dca)(tppz)(H_2O)_{0.57}(MeOH)_{0.47}]$  (**4**),  $[Mn(NO_3)_2(tppz)(H_2O)]$  (**5**),  $[Mn(N_3)(NO_3)(tppz)(H_2O)]$  (**6**),  $[Mn(SCN)_2(tppz)]$  (**7**) and  $[Mn(NO_3)(dca)(tppz)]_n$  (**8**) have been obtained. The compounds were characterized by elemental analysis, IR, EPR, magnetic measurements and X-ray analysis. Two of them (**5** and **6**) have been tested as catalysts in oxidation of alcohol to aldehydes/ketones using oxone ( $2KHSO_5 \cdot KHSO_4 \cdot K_2SO_4$ ) as an oxidant under biphasic reaction conditions ( $CH_2Cl_2/H_2O$ ) and tetra-*n*-butylammonium bromide as phase transfer agent under air at room temperature and as catalysts in oxidation of sulfides to sulfoxides with UHP (urea hydrogen peroxide) as oxidant.

© 2013 Elsevier Ltd. All rights reserved.

## 1. Introduction

2,3,5,6-Tetra-(2-pyridyl)pyrazine (*tppz*), synthesized by Goodwin and Lions in 1959, was designed as an analogue of terpyridine but with the idea that it also might bridge central ions and form extended chain structures due to six potential donor sites [1]. In metal complexes *tppz* forms seven distinct binding modes illustrated in Scheme 1.

As we can see from scheme 1, *tppz* binds to a metal center in a bidentate  $\alpha$  (a) or  $\gamma$  (b), bis-bidentate  $\alpha$  (c) or  $\gamma$  (d), tris-bidentate (e), tridentate (f) or bis-tridentate (g) coordination mode, forming both mono- and polynuclear complexes with interesting electronic and magnetic properties.

The rich photophysical and redox properties associated with these complexes make them useful for analytical purposes and probes for biologically relevant molecules such as DNA. Recently, *tppz* has been examined as fluorescence sensors for series of metal ions and off-off-on switching of fluorescence depending on stepwise complex formation with *tppz* has been reported [3].

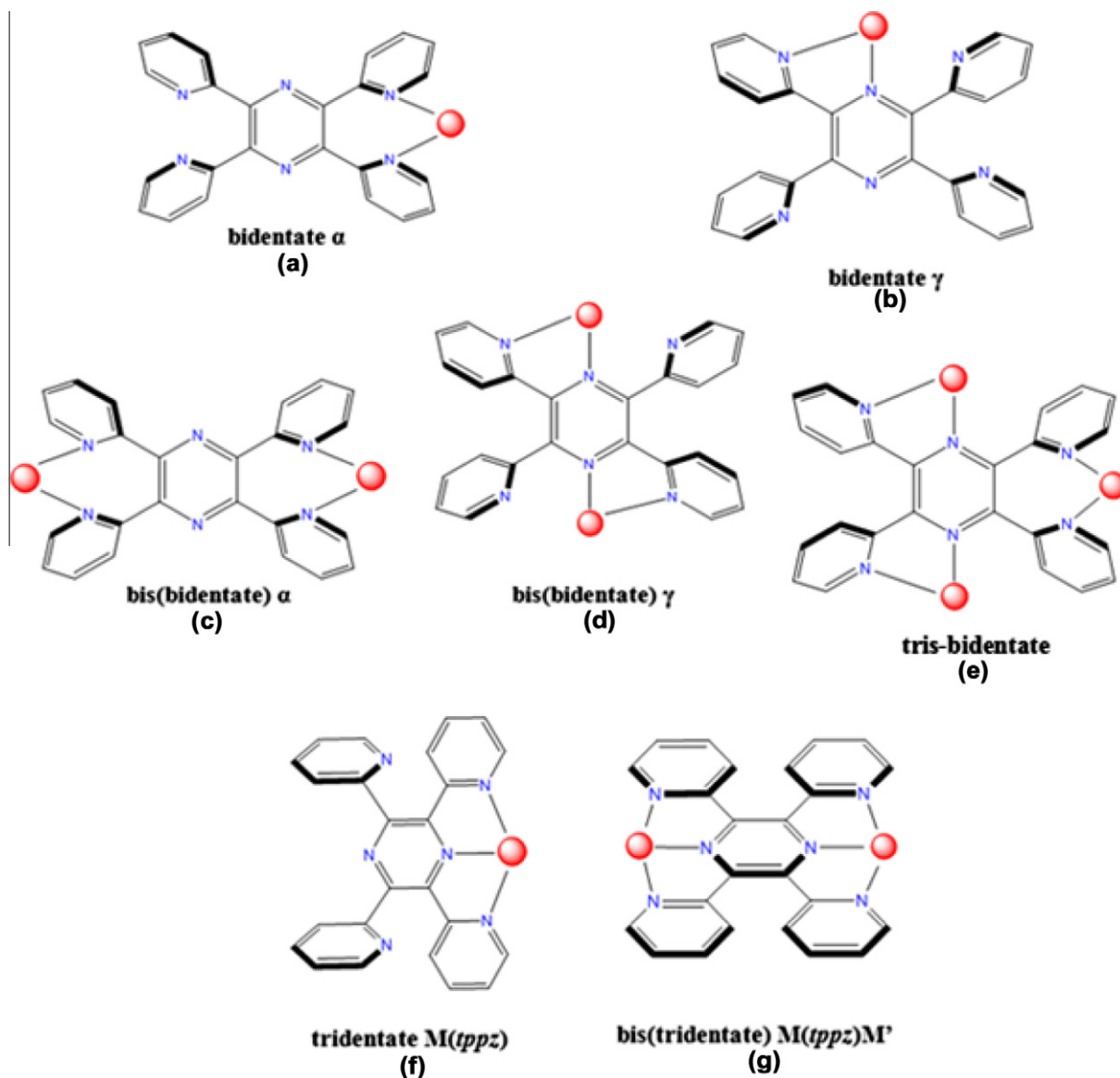
Studies on *tppz* metal(II) complexes have illustrated the ability of this polydentate organic ligand to mediate magnetic interactions

between paramagnetic centers bridged by the central pyrazine moiety and hence separated by more than 6.4 Å [4,5]. The largest antiferromagnetic interaction has been found in the dinuclear complexes  $[Cu_2(tppz)(H_2O)_4](ClO_4)_4 \cdot 2H_2O$  ( $J = -61.1 \text{ cm}^{-1}$ ) and  $[Ni_2(tppz)(H_2O)_6](NO_3)_4 \cdot 2.5H_2O$  ( $J = -76 \text{ cm}^{-1}$ ) [5]. Interestingly, the relatively good efficiency of the *tppz* bridge in transmitting magnetic interactions between paramagnetic centers contrasts with much poorer ability of unsubstituted pyrazine bridges in its metal complexes, where negligible or weak antiferromagnetic interactions were observed (with  $J$  values ranging from  $-0.14 \text{ cm}^{-1}$  in  $[Ni(py)_2Cl_2]$  to  $15.1 \text{ cm}^{-1}$  in  $Cu(py)_2(ReO_4)_2$ ) [6,7]. In binuclear ruthenium(II) complexes, *tppz* bridges have been found to mediate intermetallic electronic communication through the  $\pi$  symmetry orbitals [8]. In turn, the mononuclear complexes of Co(II) of formula  $[Co(tppz)_2]^{2+}$  with *tppz* ligands coordinated in a tridentate coordination mode attract scientific interest due to thermally induced spin crossover behaviour from a high-spin  $S_{Co} = 3/2$  at high temperatures to a low-spin  $S_{Co} = 1/2$  at lower temperatures [9].

A search in CCDC (Cambridge Crystallographic Data Centre, Version 5.33) database reveals only three Mn(II) complexes of *tppz*, namely  $[Mn_2(\mu-Cl)_2Cl_2(tppz)_2]$  [10],  $[MnI(tppz)(H_2O)_2] \cdot H_2O$  [11] and  $[Mn(dca)(NO_3)(tppz)(H_2O)]$  [12]. This prompts us to systematic studies on complex formation between Mn(II) ions, *tppz* and halide or pseudohalide ( $N_3^-$ ,  $NCS^-$  and  $N(CN)_2^-$ ) ligands. Here, we present

\* Corresponding author.

E-mail addresses: [basia@ich.us.edu.pl](mailto:basia@ich.us.edu.pl) (B. Machura), [jmroz@wchuwr.chem.uni.wroc.pl](mailto:jmroz@wchuwr.chem.uni.wroc.pl) (J. Mroziński), [rafal.kruszynski@p.lodz.pl](mailto:rafal.kruszynski@p.lodz.pl) (R. Kruszynski).



Scheme 1.

synthesis, X-ray studies as well as spectroscopic and magnetic properties of manganese(II) complexes  $[\text{Mn}_2(-\text{Cl})_2\text{Cl}_2(\text{tppz})_2]$  (**1**),  $[\text{Mn}_2\text{Cl}_2(\mu\text{-N}_3\text{-}\kappa\text{N1})_2(\text{tppz})_2]$  (**2**),  $[\text{MnCl}(\text{SCN})(\text{tppz})(\text{H}_2\text{O})]\cdot\text{H}_2\text{O}$  (**3**),  $[\text{MnCl}(\text{dca})(\text{tppz})(\text{H}_2\text{O})_{0.57}(\text{MeOH})_{0.47}]$  (**4**),  $[\text{Mn}(\text{NO}_3)_2(\text{tppz})(\text{H}_2\text{O})]$  (**5**),  $[\text{Mn}(\text{N}_3)(\text{NO}_3)(\text{tppz})(\text{H}_2\text{O})]$  (**6**),  $[\text{Mn}(\text{SCN})_2(\text{tppz})]$  (**7**) and  $[\text{Mn}(\text{NO}_3)(\text{dca})(\text{tppz})]_n$  (**8**). The molecular structure of **1** have been previously determined by Kwang [10], but the compound presented here has different conformation of the side pyridine rings and different crystal packing as compared to the literature-known one. Because the structural differences affect the magnetic properties, the contemporary structural data of **1** was included into study.

Two of these compounds (**5** and **6**) have been tested as catalysts in oxidation of alcohol to aldehydes/ketones using oxone ( $2\text{KHSO}_5\cdot\text{KHSO}_4\cdot\text{K}_2\text{SO}_4$ ) as an oxidant under biphasic reaction conditions ( $\text{CH}_2\text{Cl}_2/\text{H}_2\text{O}$ ) and tetra-*n*-butylammonium bromide as phase transfer agent under air at room temperature and as catalysts in oxidation of sulfides to sulfoxides with UHP (urea hydrogen peroxide) as oxidant. Selective oxidation of alcohols and sulfides, respectively to aldehydes/ketones and sulfoxides is a prominent reaction in laboratory and industrial synthetic chemistry [13]. In view of their importance as intermediates in organic synthesis, several

methods are available to effect this conversion, and continuous attention is drawn to newer and more selective methods of oxidation [14]. Recently, some metal complexes with N-donor ligands were used as catalysts in these reactions [15].

## 2. Experimental

*tppz* and the other reagents used to the syntheses were commercially available (POCh and Aldrich) and were used without further purification. IR spectra were recorded on a Nicolet Magna 560 spectrometer in the spectral range  $4000\text{--}400\text{ cm}^{-1}$  with the samples in the form of KBr pellets.

### 2.1. Preparation of $[\text{Mn}_2(\mu\text{-Cl})_2\text{Cl}_2(\text{tppz})_2]$ (**1**) and $[\text{Mn}(\text{NO}_3)_2(\text{tppz})(\text{H}_2\text{O})]$ (**5**)

*tppz* was dissolved in a mixture of methanol/acetonitrile (30/60 ml) and slowly added to methanolic solution of  $\text{MnCl}_2\cdot 4\text{H}_2\text{O}$  or  $\text{Mn}(\text{NO}_3)_2\cdot 4\text{H}_2\text{O}$ , and stirred at room temperature for 12 h. The

resulting solution was allowed to evaporate at room temperature and crystals of **1** and **5** were obtained after several days.

#### 2.1.1. (1) $[Mn_2(\mu-Cl)_2Cl_2(tppz)_2]$

The compound was prepared by employing  $MnCl_2 \cdot 4H_2O$  (0.2 g, 1 mmol) and *tppz* (0.39 g, 1 mmol). Yield 75% (390 mg).

Calc. for  $C_{48}H_{32}Cl_4Mn_2N_{12}$ : C, 56.05; H, 3.14; N, 16.34. Found: C, 56.34; H, 3.08; N, 16.52%.

IR (KBr,  $cm^{-1}$ ): 1631 (w), 1594 (s), 1567 (sh) and 1536 (w)  $\nu(C=N)$  and  $\nu(C=C)$ .

#### 2.1.2. (5) $[Mn(NO_3)_2(tppz)(H_2O)]$

The compound was prepared by employing  $Mn(NO_3)_2 \cdot 4H_2O$  (0.2 g, 0.8 mmol) and *tppz* (0.31 g, 0.8 mmol). Yield 70% (327 mg).

Calc. for  $C_{24}H_{18}MnN_8O_7$ : C, 49.24; H, 3.10; N, 9.38. Found: C, 49.96; H, 3.21; N, 9.81%.

IR (KBr,  $cm^{-1}$ ): 3415 (br)  $\nu(OH)$  1666 (w), 1639 (w), 1590 (m) and 1574 (sh)  $\nu(C=N)$  and  $\nu(C=C)$ .

### 2.2. Preparation of $[Mn_2Cl_2(\mu-N_3-kN1)_2(tppz)_2]$ (**2**), $[MnCl(SCN)(tppz)(H_2O)] \cdot H_2O$ (**3**), $[MnCl(dca)(tppz)(H_2O)_{0.57}(MeOH)_{0.47}]$ (**4**), $[Mn(N_3)(NO_3)(tppz)(H_2O)]$ (**6**), $[Mn(SCN)_2(tppz)]$ (**7**) and $[Mn(NO_3)(dca)(tppz)]_n$ (**8**)

$NaN_3$ ,  $NH_4SCN$  or  $NaN(CN)_2$  was dissolved in methanol and slowly added to yellow methanol/acetonitrile solution of *tppz* and  $MnCl_2$ /or  $Mn(NO_3)_2$ , and stirred at room temperature for 12 h. The resulting solution was allowed to evaporate at room temperature. Crystals, suitable for X-ray analysis, were obtained after several days.

#### 2.2.1. (2) $[Mn_2Cl_2(\mu-N_3-kN1)_2(tppz)_2]$

The compound was prepared by employing  $NaN_3$  (0.13 g, 2 mmol),  $MnCl_2 \cdot 4H_2O$  (0.2 g, 1 mmol) and *tppz* (0.39 g, 1 mmol). Yield 75% (395 mg).

Calc. for  $C_{48}H_{32}Cl_2Mn_2N_{18}$ : C, 55.35; H, 3.10; N, 24.20. Found: C, 55.92; H, 3.16; N, 24.76%.

IR (KBr,  $cm^{-1}$ ): 2065 (vs)  $\nu_{as}(N_3)$  1639 (w), 1590 (s), 1569 (sh) and 1536 (w)  $\nu(C=N)$  and  $\nu(C=C)$ .

#### 2.2.2. (3) $[MnCl(SCN)(tppz)(H_2O)] \cdot H_2O$

The compound was prepared by employing  $NH_4SCN$  (0.15 g, 2 mmol),  $MnCl_2 \cdot 4H_2O$  (0.2 g, 1 mmol) and *tppz* (0.39 g, 1 mmol). Yield 75% (434 mg).

Calc. for  $C_{25}H_{20}ClMnN_7O_2S$ : C, 52.41; H, 3.52; N, 17.11. Found: C, 51.99; H, 3.76; N, 17.81.

IR (KBr,  $cm^{-1}$ ): 3391 (br)  $\nu(O-H)$  2063 (vs)  $\nu(C=N_{SCN})$  1649 (m), 1598 (s), 1569 (sh) and 1539 (w)  $\nu(C=N)$  and  $\nu(C=C)$ .

#### 2.2.3. (4) $[MnCl(dca)(tppz)(H_2O)_{0.57}(MeOH)_{0.47}]$

The compound was prepared by employing  $NaN(CN)_2$  (0.18 g, 2 mmol),  $MnCl_2 \cdot 4H_2O$  (0.2 g, 1 mmol) and *tppz* (0.39 g, 1 mmol). Yield 65% (374 mg).

Calc. for  $C_{26.47}H_{18.94}ClMnN_9O$ : C, 55.82; H, 3.35; N, 22.14. Found: C, 55.49; H, 3.42; N, 22.65%.

IR (KBr,  $cm^{-1}$ ): 3395 (m), 3324 (m) and 3209 (m)  $\nu(O-H)$ , 2299, 2228  $\nu_s(C=)$  and 2176  $\nu_{as} + \nu_s(C=)$  1620 (m), 1601 (s), 1578 (s) and 1540 (m)  $\nu(C=N)$  and  $\nu(C=C)$ .

#### 2.2.4. (6) $[Mn(N_3)(NO_3)(tppz)(H_2O)]$

The compound was prepared by employing  $NaN_3$  (0.10 g, 1.6 mmol),  $Mn(NO_3)_2 \cdot 4H_2O$  (0.2 g, 1 mmol) and *tppz* (0.31 g, 0.8 mmol). Yield 65% (293 mg).

Calc. for  $C_{24}H_{18}MnN_{10}O_4$ : C, 50.98; H, 3.21; N, 9.72. Found: C, 50.17; H, 3.30; N, 9.99%.

IR (KBr,  $cm^{-1}$ ): 3394 (br)  $\nu(O-H)$  2061 (vs)  $\nu_{as}(N_3)$  1631 (w), 1594 (s), 1570 (sh) and 1534 (w)  $\nu(C=N)$  and  $\nu(C=C)$ .

#### 2.2.5. (7) $[Mn(SCN)_2(tppz)]$

The compound was prepared by employing  $NH_4SCN$  (0.10 g, 1.6 mmol),  $Mn(NO_3)_2 \cdot 4H_2O$  (0.2 g, 0.8 mmol) and *tppz* (0.31 g, 0.8 mmol). Yield 75% (334 mg).

Calc. for  $C_{26}H_{16}MnN_8S_2$ : C, 55.81; H, 2.88; N, 20.03. Found: C, 55.21; H, 3.01; N, 20.69%.

IR (KBr,  $cm^{-1}$ ): 2048 (vs)  $\nu(C=N_{SCN})$  1642 (w), 1588 (s), 1567 (sh)  $\nu(C=N)$  and  $\nu(C=C)$ .

#### 2.2.6. (8) $[Mn(NO_3)(dca)(tppz)]_n$

The compound was prepared by employing  $NaN(CN)_2$  (0.14 g, 1.6 mmol),  $Mn(NO_3)_2 \cdot 4H_2O$  (0.2 g, 0.8 mmol) and *tppz* (0.31 g, 0.8 mmol). Yield 70% (319 mg).

Calc. for  $C_{26}H_{16}MnN_{10}O_3$ : C, 54.65; H, 2.82; N, 24.51. Found: C, 54.10; H, 2.92; N, 24.98%.

IR (KBr,  $cm^{-1}$ ): 2310  $\nu_s(C=N)$  and 2172  $\nu_{as} + \nu_s(C=N)$  1590 (s), 1568 (sh) and 1537 (w)  $\nu(C=N)$  and  $\nu(C=C)$ .

### 2.3. Crystal structures determination and refinement

The X-ray intensity data of **1–8** were collected on a Gemini A Ultra diffractometer equipped with Atlas CCD detector and graphite monochromated Mo  $K\alpha$  radiation ( $\lambda = 0.71073 \text{ \AA}$ ) at room temperature. Details concerning crystal data and refinement are given in Table 1. Lorentz, polarization and empirical absorption correction using spherical harmonics implemented in SCALE3 ABSPACK scaling algorithm [16] were applied. The structures were solved by the direct methods and subsequently completed by the difference Fourier recycling. All the non-hydrogen atoms were refined anisotropically using full-matrix, least-squares technique. The hydrogen atoms were treated as “riding” on their parent carbon atoms and assigned isotropic temperature factors equal 1.2 (aromatic) and 1.5 (water) times the value of equivalent temperature factor of the parent atom. The methyl groups were allowed to rotate about their local threefold axis. SHELXS97 and SHELXL97 [17] programs were used for all the calculations. Atomic scattering factors were those incorporated in the computer programs. At  $x$ ,  $\frac{1}{2}$ ,  $\frac{1}{2}$  the compound **1** have the solvent accessible void of about  $180 \text{ \AA}^3$ , filled with the continuous electron density not larger than  $0.377 \text{ e \AA}^{-3}$ . Because such density do not show any clear maximum it can be stated that above mentioned solvent accessible void is filled with the diffused solvent (multiple, differently disordered solvent molecules). Refinement of the model which does not comprise the diffused solvent leads to the satisfactory and reasonable structural parameters (Table 1). The compound **4** contains build up into the inner coordination sphere the disorder solvent molecules (water/methanol). These solvents exist almost alternately in the crystal net molecules and the oxygen atoms of both molecules occupy almost equivalent places in the asymmetric unit.

### 2.4. Magnetic measurement and EPR spectra

Variable-temperature magnetic measurements of polycrystalline samples were carried out with a Quantum Design SQUID magnetometer (MPMSXL-5-type) at a magnetic field of 0.5 T over the temperature range 1.8–300 K. Correction are based on subtracting the sample-holder signal, contribution  $\chi_{Dia}$  estimated from Pascal constants [18]. The effective magnetic moment was calculated from the equation:  $\mu_{eff} = 2.83(\chi_M T)^{1/2}$  (B.M.). Magnetization versus magnetic field measurements were carried out at 2 K in the magnetic field range 0–5 T.

EPR spectra were recorded at room temperature and 77 K on a Brüker ESP 300 spectrometer operating at X-band, equipped with

**Table 1**  
Crystal data and structure refinement for 1–8.

	1	2	3	4	5	6	7	8
Empirical formula	C <sub>48</sub> H <sub>32</sub> Cl <sub>4</sub> Mn <sub>2</sub> N <sub>12</sub>	C <sub>48</sub> H <sub>32</sub> Cl <sub>2</sub> Mn <sub>2</sub> N <sub>18</sub>	C <sub>25</sub> H <sub>20</sub> ClMnN <sub>7</sub> O <sub>2</sub> S	C <sub>26.47</sub> H <sub>18.94</sub> ClMnN <sub>9</sub> O	C <sub>24</sub> H <sub>18</sub> MnN <sub>8</sub> O <sub>7</sub>	C <sub>24</sub> H <sub>18</sub> MnN <sub>10</sub> O <sub>4</sub>	C <sub>26</sub> H <sub>16</sub> MnN <sub>8</sub> S <sub>2</sub>	C <sub>26</sub> H <sub>16</sub> MnN <sub>10</sub> O <sub>3</sub>
Formula weight	1028.54	1041.70	572.93	569.51	585.40	565.42	559.53	571.43
Temperature (K)	293.0(2)	293.0(2)	293.0(2)	293.0(2)	293.0(2)	293.0(2)	293.0(2)	293.0(2)
Wavelength (Å)	0.71073	0.71073	0.71073	0.71073	0.71073	0.71073	0.71073	0.71073
Crystal system	triclinic	triclinic	monoclinic	monoclinic	monoclinic	monoclinic	monoclinic	monoclinic
Space group	<i>P</i> $\bar{1}$	<i>P</i> $\bar{1}$	<i>P</i> 2 <sub>1</sub> / <i>n</i>	<i>P</i> 2 <sub>1</sub> / <i>c</i>	<i>P</i> 2 <sub>1</sub> / <i>n</i>	<i>P</i> 2 <sub>1</sub> / <i>c</i>	<i>P</i> 2 <sub>1</sub> / <i>n</i>	<i>P</i> 2 <sub>1</sub> / <i>n</i>
<i>Unit cell dimensions</i>								
<i>a</i> (Å)	9.3470(5)	8.9184(4)	17.1955(14)	15.8314(8)	14.3966(5)	14.0217(5)	15.8687(6)	9.3542(5)
<i>b</i> (Å)	10.4400(6)	11.0500(5)	7.3436(6)	7.3101(5)	9.5914(4)	9.7158(4)	7.3574(2)	8.7838(3)
<i>c</i> (Å)	13.4185(8)	13.0981(6)	21.7739(18)	22.4617(9)	18.6066(7)	22.4628(8)	22.3087(8)	31.2293(14)
$\alpha$ (°)	72.537(5)	107.895(4)						
$\beta$ (°)	78.073(5)	96.332(3)	110.744(9)	99.942(4)	94.362(3)	123.700(3)	108.884(4)	97.324(4)
$\gamma$ (°)	81.714(5)	105.086(4)						
Volume (Å <sup>3</sup> )	1217.36(12)	1160.31(9)	2571.3(4)	2560.4(2)	2561.82(17)	2545.91(17)	2464.41(15)	2545.0(2)
<i>Z</i>	1	1	4	4	4	4	4	4
Density (calculated) (Mg/m <sup>3</sup> )	1.403	1.491	1.480	1.477	1.518	1.475	1.508	1.491
Absorption coefficient (mm <sup>-1</sup> )	0.785	0.717	0.736	0.660	0.576	0.571	0.738	0.569
<i>F</i> (000)	522	530	1172	1163	1196	1156	1140	1164
Crystal size (mm)	0.025 × 0.109 × 0.261	0.025 × 0.067 × 0.242	0.255 × 0.135 × 0.090	0.017 × 0.072 × 0.185	0.028 × 0.049 × 0.170	0.047 × 0.085 × 0.102	0.074 × 0.160 × 0.254	0.031 × 0.106 × 0.250
$\theta$ range for data collection (°)	3.47–25.00	3.44–25.00	3.39–25.05	3.45–25.05	3.44–25.05	3.44–25.05	3.40–25.00	3.51–25.05
Index ranges	–11 ≤ <i>h</i> ≤ 10 –12 ≤ <i>k</i> ≤ 12 –15 ≤ <i>l</i> ≤ 14	–10 ≤ <i>h</i> ≤ 10 –13 ≤ <i>k</i> ≤ 12 –15 ≤ <i>l</i> ≤ 15	–20 ≤ <i>h</i> ≤ 20 –8 ≤ <i>k</i> ≤ 8 –25 ≤ <i>l</i> ≤ 25	–18 ≤ <i>h</i> ≤ 18 –7 ≤ <i>k</i> ≤ 8 –26 ≤ <i>l</i> ≤ 25	–17 ≤ <i>h</i> ≤ 17 –11 ≤ <i>k</i> ≤ 10 –22 ≤ <i>l</i> ≤ 22	–16 ≤ <i>h</i> ≤ 16 –11 ≤ <i>k</i> ≤ 11 –26 ≤ <i>l</i> ≤ 26	–18 ≤ <i>h</i> ≤ 18 –8 ≤ <i>k</i> ≤ 8 –20 ≤ <i>l</i> ≤ 26	–9 ≤ <i>h</i> ≤ 11 –10 ≤ <i>k</i> ≤ 10 –37 ≤ <i>l</i> ≤ 29
Reflections collected	8285	8814	14670	11993	14432	13646	10633	11263
Independent reflections	4273 ( <i>R</i> <sub>int</sub> = 0.0354)	4077 ( <i>R</i> <sub>int</sub> = 0.0326)	4546 ( <i>R</i> <sub>int</sub> = 0.0425)	4525 ( <i>R</i> <sub>int</sub> = 0.0426)	4532 ( <i>R</i> <sub>int</sub> = 0.0523)	4512 ( <i>R</i> <sub>int</sub> = 0.0582)	4327 ( <i>R</i> <sub>int</sub> = 0.0214)	4503 ( <i>R</i> <sub>int</sub> = 0.0312)
Completeness to 2 $\theta$ (%)	99.7	99.7	99.8	99.8	99.7	99.8	99.7	99.7
Min. and max. transm. Data/restraints/parameters	0.812 and 1.000 4273/0/298	0.903 and 1.000 4077/0/316	0.712 and 1.000 4546/7/334	0.772 and 1.000 4525/0/362	0.856 and 1.000 4532/0/361	0.927 and 1.000 4512/0/354	0.766 and 1.000 4327/0/334	0.937 and 1.000 4503/0/361
Goodness-of-fit on <i>F</i> <sup>2</sup>	0.941	1.028	1.072	1.028	0.980	1.110	1.045	1.036
Final <i>R</i> indices [ <i>I</i> > 2 $\sigma$ ( <i>I</i> )]	<i>R</i> <sub>1</sub> = 0.0478 <i>wR</i> <sub>2</sub> = 0.1128	<i>R</i> <sub>1</sub> = 0.0446 <i>wR</i> <sub>2</sub> = 0.1046	<i>R</i> <sub>1</sub> = 0.0561 <i>wR</i> <sub>2</sub> = 0.1499	<i>R</i> <sub>1</sub> = 0.0436 <i>wR</i> <sub>2</sub> = 0.0958	<i>R</i> <sub>1</sub> = 0.0498 <i>wR</i> <sub>2</sub> = 0.1055	<i>R</i> <sub>1</sub> = 0.0461 <i>wR</i> <sub>2</sub> = 0.1330	<i>R</i> <sub>1</sub> = 0.0340 <i>wR</i> <sub>2</sub> = 0.0886	<i>R</i> <sub>1</sub> = 0.0387 <i>wR</i> <sub>2</sub> = 0.0883
<i>R</i> indices (all data)	<i>R</i> <sub>1</sub> = 0.0764 <i>wR</i> <sub>2</sub> = 0.1227	<i>R</i> <sub>1</sub> = 0.0701 <i>wR</i> <sub>2</sub> = 0.1144	<i>R</i> <sub>1</sub> = 0.0737 <i>wR</i> <sub>2</sub> = 0.1629	<i>R</i> <sub>1</sub> = 0.0841 <i>wR</i> <sub>2</sub> = 0.1055	<i>R</i> <sub>1</sub> = 0.0864 <i>wR</i> <sub>2</sub> = 0.1155	<i>R</i> <sub>1</sub> = 0.0828 <i>wR</i> <sub>2</sub> = 0.1422	<i>R</i> <sub>1</sub> = 0.0490 <i>wR</i> <sub>2</sub> = 0.0917	<i>R</i> <sub>1</sub> = 0.0562 <i>wR</i> <sub>2</sub> = 0.0943
Largest diff. peak and hole (e Å <sup>-3</sup> )	0.377 and –0.354	0.440 and –0.472	0.743 and –0.460	0.420 and –0.259	0.654 and –0.365	1.039 and –0.242	0.407 and –0.587	0.655 and –0.382

an ER 035M Brüker NMR gaussmeter and HP 5350B Hewlett–Packard microwave frequency counter.

## 2.5. Catalytic studies

### 2.5.1. General procedure in oxidation of alcohol

In a typical experiment, a solution of Oxone (0.2 mmol) in H<sub>2</sub>O (5 ml) at room temperature was added to a solution of alcohol (0.2 mmol), tetra-*n*-butylammonium bromide, (0.1 mmol), and catalyst (0.01 mmol), in CH<sub>2</sub>Cl<sub>2</sub> (1 mL), and the biphasic mixture stirred vigorously. Formation of products and consumption of substrates were monitored by gas chromatography. The identity of products was determined by comparison with authentic samples using gas–liquid chromatography. Oxidation products yields based on the oxidant, were quantified by comparison with chlorobenzene.

### 2.5.2. General procedure for sulfide oxidation

To a solution of sulfide (0.2 mmol), imidazole (0.1 mmol) as axial ligand, chlorobenzene (0.2 mmol) as internal standard and catalyst (0.01 mmol) in a (1:1) mixture of CH<sub>3</sub>OH/CH<sub>2</sub>Cl<sub>2</sub> (1 ml) was added UHP (0.4 mmol) as oxidant. The mixture was stirred at room temperature and the progress of the reaction was monitored by GC, by removing small samples of the reaction mixture. To establish the identity of the products unequivocally, the retention times and spectral data were compared to those of commercially available compounds.

## 3. Results and discussion

### 3.1. Preparation and infrared data

The preparations of complexes **1–8** were carried out in a mixture methanol–acetonitrile in molar ratio of manganese(II) ions to ligand equal 1:1, and two manganese(II) salts (MnCl<sub>2</sub>·4H<sub>2</sub>O and Mn(NO<sub>3</sub>)<sub>2</sub>·4H<sub>2</sub>O) were used for the syntheses. The reaction of *tpz* with MnCl<sub>2</sub> yields [Mn<sub>2</sub>(μ-Cl)<sub>2</sub>(*tpz*)<sub>2</sub>] (**1**), while Mn(NO<sub>3</sub>)<sub>2</sub> reacts with *tpz* to form [Mn(NO<sub>3</sub>)<sub>2</sub>(*tpz*)(H<sub>2</sub>O)] (**5**). Interestingly, the choice of manganese(II) salt turned out to be crucial in complex formation with *tpz* and pseudohalide ligands. MnCl<sub>2</sub> reacts with *tpz* and NH<sub>4</sub>SCN, NaN<sub>3</sub> or NaN(CN)<sub>2</sub> to give [MnCl(SCN)(*tpz*)(H<sub>2</sub>O)]·H<sub>2</sub>O (**3**), [Mn<sub>2</sub>Cl<sub>2</sub>(μ-N<sub>3</sub>-kN1)<sub>2</sub>(*tpz*)<sub>2</sub>] (**2**) and [MnCl(dca)(*tpz*)(H<sub>2</sub>O)<sub>0.57</sub>(MeOH)<sub>0.47</sub>] (**4**), respectively, whereas the reactions of Mn(NO<sub>3</sub>)<sub>2</sub> with *tpz* and NH<sub>4</sub>SCN, NaN<sub>3</sub> or NaN(CN)<sub>2</sub> yield [Mn(SCN)<sub>2</sub>(*tpz*)] (**7**), [Mn(N<sub>3</sub>)(NO<sub>3</sub>)(*tpz*)(H<sub>2</sub>O)] (**6**) and [Mn(NO<sub>3</sub>)(dca)(*tpz*)<sub>*n*</sub>] (**8**).

In high frequency region the IR spectra of **3**, **4**, **5** and **6** show broad and strong absorptions centered at 3391 cm<sup>-1</sup> for **3**, 3395, 3324 and 3209 cm<sup>-1</sup> for **4**, 3415 cm<sup>-1</sup> for **5** and 3394 cm<sup>-1</sup> for **6**, assignable to the O–H stretching water molecules. Intense absorptions associated with the stretching modes of the pseudohalide ions occur at 2065 cm<sup>-1</sup> for **2**, 2063 cm<sup>-1</sup> for **3**, 2299, 2228 and 2176 cm<sup>-1</sup> for **4**, 2061 cm<sup>-1</sup> for **6**, 2048 cm<sup>-1</sup> for **7**, 2310 and 2172 cm<sup>-1</sup> for **8**. Peaks revealing the presence of *tpz* occur in the ranges 3100–2880 cm<sup>-1</sup> (aromatic C–H stretching vibrations), 1600–1530 cm<sup>-1</sup> (ν(C=N) and ν(C=C) stretches), 1480–1000 cm<sup>-1</sup> (ν(C–C) + ν(C–N) vibrations) and 800–700 cm<sup>-1</sup> (aromatic C–H deformation vibrations). In the case of **5**, **6** and **8** the region 1480–1000 cm<sup>-1</sup> is partially obscured by the strong nitrate NO<sub>3</sub><sup>-</sup> stretching modes [19].

### 3.2. Crystal structure analysis

The crystallographic data of **1–8** are summarized in Table 1.

The intra- and intermolecular contacts [20] detected in the structures **2–8** are collected in Table S1. The compound **1** does not show any interaction which can be classified even as weak hydrogen bond, however, due to existence of diffused solvent in the crystal structure, the intermolecular contacts scheme is incomplete and some bonding interactions between the solvent and complex molecules eventually may exist. It can be postulated that formation of the hydrogen bond between the solvent and complex molecules leads to stabilization of the solvent molecules positions in the crystal structure, thus the presence of diffused solvent may indicated a lack of the intermolecular interactions between the solvent and complex molecules. The molecules of compounds **2**, **7** and **8** are interconnected only by weak C–H···D hydrogen bonds (Table S1), respectively, to the chains extending along the crystallographic [011] axis, to the dimers and to the ribbons exiting along the crystallographic [010] axis and perpendicular to the crystallographic (013) plane. The complex molecules of **3** are connected by O–H···Cl medium strength hydrogen bonds to the chains extending along crystallographic [010] axis and described C(4) graph. The unitary graph set is formed by these C(4) motifs and additional D motifs of O–H···O hydrogen bonds. The weak C–H···Cl hydrogen bonds (Table S1) expands above mentioned chains to the layers propagating along crystallographic (10 $\bar{1}$ ) plane, and weak C–H···S hydrogen bonds (Table S1) extends these layers to the 3D supramolecular network. The molecules of **4** are linked to hydrogen bonded dimers by O–H···N interactions forming N<sub>1</sub>C<sub>2</sub><sup>2</sup>(16) motifs. The presence of the weak C–H···Cl hydrogen bonds lead to formation of the 3D network in **4**. The medium strength O–H···A hydrogen bonds link the molecules of **5** to the chains extending along crystallographic [010] axis and described by C(4)C(6)C(8) basic unitary graph set motifs. The weak C–H···O hydrogen bonds expands these chains to the 3D supramolecular network. In compound **6**, similarly to the **5**, the O–H···N hydrogen bonds extends molecules to the chains located along crystallographic [010] axis but they forms the C(4)C(5)C(8) basic unitary graph set. Additionally the weak C–H···O hydrogen bonds present in **6** link above mentioned chain to the plane expanding along the crystallographic (001) plane. Additionally the molecules of the compounds **2–6** and **8** are internally linked by the by the weak C–H···A intramolecular bonds.

### 3.3. [Mn<sub>2</sub>(-Cl)<sub>2</sub>Cl<sub>2</sub>(*tpz*)<sub>2</sub>] (**1**) and [Mn<sub>2</sub>Cl<sub>2</sub>(-N<sub>3</sub>-N1)<sub>2</sub>(*tpz*)<sub>2</sub>] (**2**)

Compounds **1** and **2** crystallize in the triclinic space group *P* $\bar{1}$ . Perspective view of the molecule **2** with the labeling of the atoms are depicted in Fig. 1, and the relevant bond lengths of **1** and **2** are collected in Table 2. The molecular structure of **1** and detailed structural parameters of **1** and **2** were included in Supplementary materials (Fig. S1, Tables S2 and S3). The dinuclear complexes **1** and **2** result from the pairing of two mononuclear units related by a crystallographic center of inversion. In **1** the manganese(II) centers are doubly bridged by chloride ions, whereas the Mn(II) of **2** are doubly linked by *end-on* (EO) azide groups.

In both dimers, the four atoms involved in bridging form a perfect plane due to the existence of an inversion center. The resulting intradimeric Mn···Mn separation of 3.859 Å in **1** and 3.553 Å in **2** falls in the range reported for the related Mn(II) dimers [21]. Similarly, the bridging angles Mn(1)–Cl(2)–Mn(1)#1 (96.59(3)°) and Mn(1)–N(99)–Mn(1)#1 (104.91(11)°) are in good agreement with data reported in the literature, for example in [MnCl(μ-Cl)(mpbpa)]<sub>2</sub> the Mn(1)–Cl(1)–Mn(1)<sup>i</sup> angle equals 94.426(19)° [21a] and in [Mn(terpy)(N<sub>3</sub>)<sub>2</sub>]·2H<sub>2</sub>O the Mn–N<sub>4</sub>–Mn<sup>i</sup> angle is 104.6(1)° [21e]. The two Mn<sub>2</sub>Cl bridging bond lengths in **1** are significantly different (2.4227(10) Å and 2.7391 Å). A similar trend is observed in **2**, where Mn–N corresponding to the bridging azide groups are equal 2.161(2) and 2.319(3) Å.

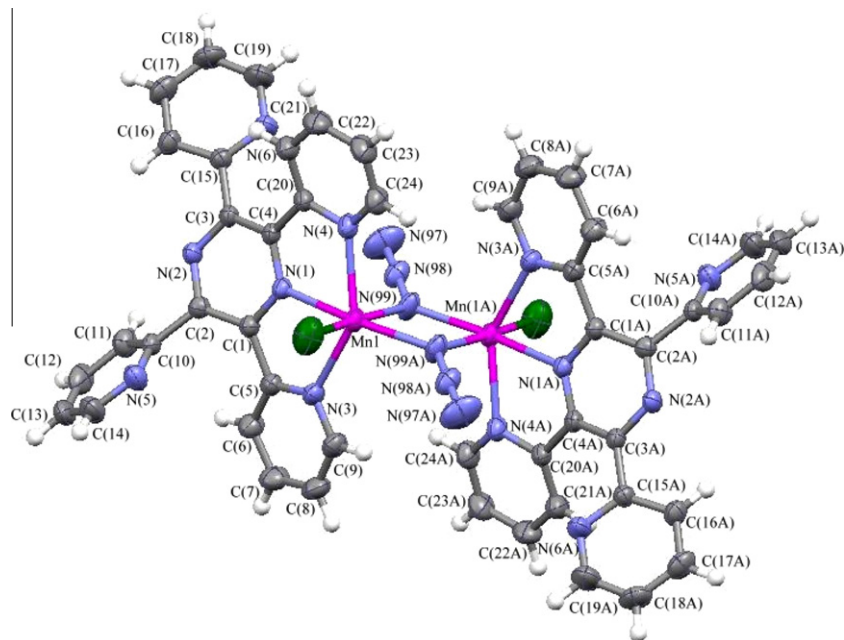


Fig. 1. The molecular structure of **2**. Displacement ellipsoids are drawn at 50% probability.

Table 2

The relevant bond lengths of **1–8**.

	<b>1</b>	<b>2</b>	<b>3</b>	<b>4</b>	<b>5</b>	<b>6</b>	<b>7</b>	<b>8</b>
Mn–N <sub>ppz</sub>	2.243(3)	2.275(2)	2.224(2)	2.248(2)	2.267(2)	2.283(2)	2.2455(17)	2.3096(18)
Mn–N(3) <sub>py</sub>	2.255(3)	2.254(2)	2.243(3)	2.256(2)	2.316(2)	2.327(3)	2.2423(17)	2.2701(19)
Mn–N(4) <sub>py</sub>	2.265(3)	2.275(3)	2.235(3)	2.226(2)	2.295(2)	2.293(3)	2.2432(18)	2.3212(19)
Mn–Cl(1)	2.4461(10)	2.4266(11)	2.5009(13)	2.4763(11)				
Mn–Cl(2)	2.7391(10)							
Mn–N <sub>azide</sub>		2.161(2)				2.200(3)		
Mn–N(99) <sub>SCN<sup>−</sup></sub>			2.060(3)				2.156(2)	
Mn–N(98) <sub>SCN<sup>−</sup></sub>							2.032(2)	
Mn–O <sub>water</sub>			2.465(4)	2.294(13)	2.160(2)	2.183(2)		2.367(2)
Mn–O <sub>MeOH</sub>				2.19(2)				
Mn–O(1) <sub>nitrate</sub>					2.317(3)	2.298(3)		2.295(2)
Mn–O(2) <sub>nitrate</sub>					2.372(2)	2.407(3)		
Mn–O(4) <sub>nitrate</sub>					2.238(3)			
Mn–N(99) <sub>dca</sub>				2.108(3)				2.201(2)
Mn–N(97) <sub>dca</sub>								2.2292(19)

Each Mn(II) ion in the two dimers exhibits a distorted octahedral coordination sphere. The main source of distortion of the metal surrounding comes from the bites taken by *tppz* ligand equal 71.04(9)° and 71.48(10)° for **1** and 70.11(8)° and 71.56(8)° for **2**. In complex **1** the Mn(1) ions are coordinated by three N atoms from the *tppz* ligand and three chloride ligands giving a six-coordinate *mer*-N<sub>3</sub>Cl<sub>3</sub> donor set. In **2** three nitrogen atoms of the *tppz* ligand and one nitrogen atom of end-on azido ligand act as the equatorial plane, while the nitrogen atom of the second *end-on* azido ligand and chloride ion situate in the axial positions.

The Mn–N bond lengths, ranging from 2.243(3) Å to 2.319(3) Å, and Mn–Cl distances, from 2.4227(10) to 2.7391(10) Å, fall within the normal range in dimers incorporating six-coordinate manganese(II) ions [21,22]. In **1**, the bond distance of Mn(II) to the middle nitrogen N(1) is shorter than Mn(1)–N(3) and Mn(1)–N(4) distances, which is usually observed in *tppz*-like ligands [2]. The shortness of Mn–N<sub>pyrazine</sub> distance within the *tppz* unit is attributed to a more efficient overlap of the metal *t<sub>2g</sub>* orbitals with the  $\pi^*$  orbitals of the central pyrazine ring compared to the distal pyridyl groups. This trend is not observed in complex **2**, probably due to a *trans* effect of the azide group.

The *tppz* ligand is appreciably twisted, dihedral angles between the pyrazine ring and each of the pyridyl rings are equal 41.35(12)°, 31.95(14)°, 30.03(15)° and 21.74(16)° in **1** and 51.85(10)°, 29.53(12)°, 26.77(15)° and 18.57(17)° in **2**. The pyrazine ring itself is puckered with maximum atomic deviations from a best mean plane being 0.1053 Å at C(4) in **1** and 0.0995 Å at C(2) in **2**. The torsion angles N1–C1–C2–N2 and N2–C3–C4–N1 are –18.51(41)° and 16.83(39)° in **1** and, and the dihedral angle between the two C–N–C planes of the pyrazine ring is 10.07(46)° in **1** and 5.18(33)° in **2**. The non-planarity of the pyrazine ring is unexceptional. It has been reported for the related structures [2b,c,4,6,11,23,24], and the factor responsible for destabilizing the planar geometry of the pyrazine ring has a pure electronic origin [25].

### 3.4. [MnCl(SCN)(*tppz*)(H<sub>2</sub>O)]·H<sub>2</sub>O (**3**) and [MnCl(dca)(*tppz*)(H<sub>2</sub>O)<sub>0.57</sub>(MeOH)<sub>0.47</sub>] (**4**)

A perspective view of the molecule **3** with the labeling of the atoms are depicted in Fig. 2, and the relevant bond lengths and angles of the molecule **3** and **4** are collected in Table 2. The molecular structure of **4** and detailed structural parameters of **3** and **4** were

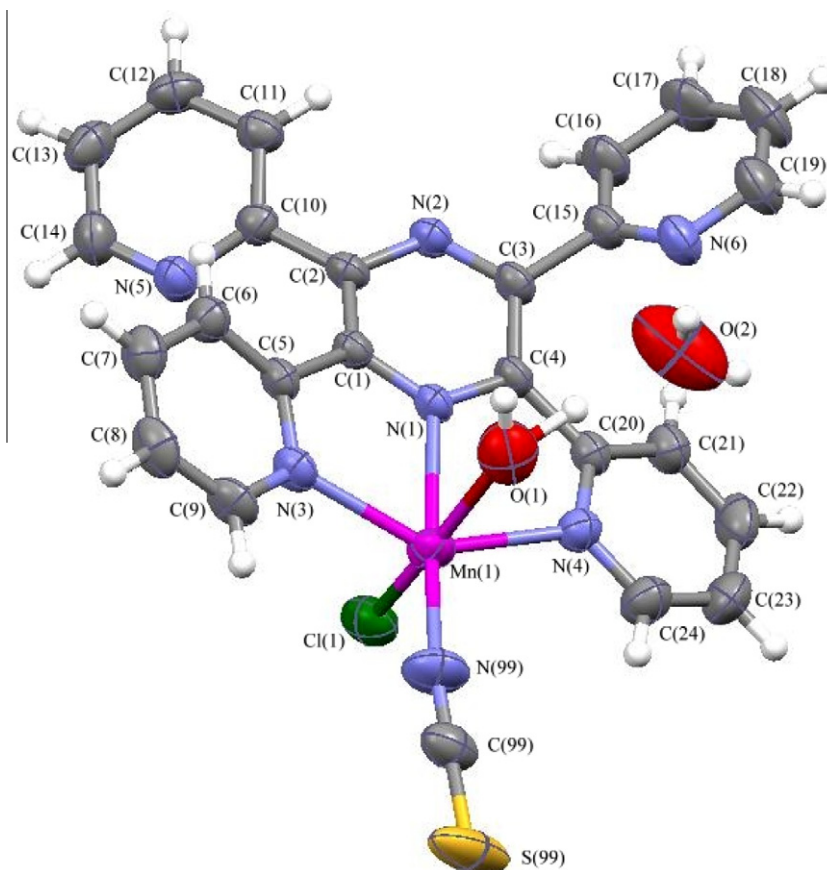


Fig. 2. The molecular structure of **3**. Displacement ellipsoids are drawn at 50% probability.

included in Supplementary materials (Fig. S2, Tables S4 and S5). In both compounds the metal center is six coordinate and shows a distorted octahedral geometry. The tridentate *tppz* ligand and pseudohalide ion (quasi-linear (178.5(4)°) terminal thiocyanate ion in **3** and *dca* anion in **4**) constitute the equatorial plane, while axial positions are occupied by chloride ion and solvent molecule.

The Mn–N bond lengths of **3** follow a decreasing order for pyridyl (2.243(3) and 2.234(3) Å), pyrazine (2.224(3) Å) and thiocyanate (2.060(3) Å) donors, indicating the expected variation in coordinating ability. The anionic NCS N-donors bind most strongly, followed by the two neutral nitrogen donors from the heterocycles.

Similar to the previous structures, there is twisting between the pyrazine and pyridyl rings. The uncoordinated pyridine rings are inclined toward the pyrazine ring by 39.13(9)°, 27.40(8)° in **3** and 39.26(8)°, 28.41(6)° in **4**, and the dihedral angles between the pyrazine ring and coordinated pyridyl rings are equal 17.59(13)° and 23.22(13)° in **3** and 19.74(12)° and 23.18(11)° in **4**. The individual pyridyl rings are planar within experimental errors, while the pyrazine ring is significantly puckered (with maximum atomic deviations from a best mean plane being 0.1113(22) Å at C(4)) in **3** and 0.1141(19) Å at C(2)) in **4**.

### 3.5. [Mn(NO<sub>3</sub>)<sub>2</sub>(*tppz*)(H<sub>2</sub>O)] (**5**) and [Mn(N<sub>3</sub>)(NO<sub>3</sub>)<sub>2</sub>(*tppz*)(H<sub>2</sub>O)] (**6**)

The manganese(II) ions of **5** and **6** are heptacoordinated with coordination polyhedron close to the pentagonal bipyramid (Figs. S3 and S4). In **5** the heptacoordination is achieved by means of three N atoms from the *tppz* ligand and two oxygen atoms from the bidentate nitrate ligand, which determine the equatorial plane, and two oxygen atoms, from the water molecule and monodentate nitrate group, in axial positions. The equatorial plane of **6** is also

constituted by three N atoms of *tppz* ligand and two oxygen atoms from the bidentate nitrate ligand, but axial positions are occupied by the oxygen atom belonging to the water molecule and nitrogen atom of the azide group. A rare heptacoordinated geometry of Mn(II) ions in **5** and **6** seems to be governed by simultaneous existence of bidentate nitrate ligand leading to the formation of four-membered chelate ring and tridentate *tppz* ligand forming with the central ion two five-membered chelate rings. The deviation from ideal pentagonal bipyramidal geometry, clearly indicated by bond angles in the equatorial plane, comes from the bites taken by the nitrate ion (54.19(8) in **5** and 54.01(8) in **6**) and *tppz* ligands (70.41(9) and 70.45(9) in **5** and 69.75(9) and 70.95(9) in **6**). In turn, the bond angles N(3)–Mn(1)–O(1) (81.60(11)°) and N(4)–Mn(1)–O(2) (85.04(11)°) are considerably greater than ideal for pentagonal bipyramidal geometry value 72°.

The individual pyridyl rings are planar within experimental errors, while the pyrazine ring is significantly puckered, with maximum atomic deviations from a best mean plane being 0.1105(20) Å at C(2) in **5** and 0.1112(21) Å at C(2) in **6**. The dihedral angles between the pyrazine and uncoordinated pyridyl rings are 38.86(13)° and 34.50(14)° in **5** and 38.60(16)° and 36.06(17)° in **6**, whereas the coordinated pyridine rings are inclined toward the pyrazine ring by 20.16(10) and 25.86(9) in **5** and 18.86(11) and 26.74(10) in **6**. The Mn–N bonds involving the *tppz* ligand vary from 2.267(2) to 2.327(3) Å, and the Mn–N distance for the coordinated pyrazine is slightly shorter in comparison with Mn–N<sub>pyridine</sub> (Tables S6 and S7).

According to the criteria introduced by Kleywegt al. [26] for determining nitrate binding mode (Table S8) the NO<sub>3</sub><sup>−</sup> group of **5** coordinates to central ion in an symmetric bidentate fashion. For complex **6** two coordination modes have been confirmed. The ni-

trate group occupying the axial position bounds to the central ion in a monodentate mode, whereas  $\text{NO}_3^-$  in the equatorial plane coordinates in symmetric bidentate fashion.

### 3.6. $[\text{Mn}(\text{SCN})_2(\text{tppz})]$ (**7**)

The molecular structure of **7** with the labeling of the atoms is depicted in Fig. S5, and the selected bond lengths and angles are collected in Table S9. The manganese(II) ion is five-coordinate by three N atoms of *tppz* ligand and two atoms of thiocyanate ions and shows square-based pyramidal geometry (SP). The equatorial plane of manganese(II), defined by three *tppz* nitrogen atoms and one nitrogen atom of the thiocyanate group, has a slight tetrahedral distortion and the metal atom is displaced by 0.317(1) Å from this plane in the direction of the apical position, occupying by the nitrogen atom of the second  $\text{SCN}^-$  ion. As in the aforementioned structures, the *tppz* ligand is appreciably twisted, the coordinated pyridine rings are inclined toward the central pyrazine by 24.89(8)° and 29.83(7)°, and dihedral angles between the pyrazine and uncoordinated pyridyl rings are 46.58(7)° and 56.78(5)°. Interestingly, the pyrazine ring in **7** is flat within experimental error (maximum atomic deviation at C(2) equals to 0.0221(14) Å).

The Mn–N, ranging from 2.032(2) to 2.4555(17) Å, are consistent with the values observed in other penta-coordinated mononuclear manganese(II) complexes [27]. The Mn–N bond length is shortest for thiocyanate nitrogens, indicating their stronger coordination than the pyridyl and pyrazine nitrogens of *tppz* ligand. Similar to the complex **2**, the bond distance of Mn(II) to the middle nitrogen N(1) is slightly longer than Mn(1)–N(3) and Mn(1)–N(4) distances, which is probably due to a *trans* effect of the thiocyanate group. The NCS groups are quasilinear with N–C–S bond angle of 178.7(3)° and 179.5(2)° and are bonded to the metal ion through an angle of 165.5(2)° and 137.2(2)°, respectively. The bent coordination is rarer compared to the linear one. Previously, it was re-

ported for  $[\text{Mn}(\text{dpka})_2(\text{NCS})_2] \cdot \frac{1}{2}\text{H}_2\text{O}$  ( $\angle\text{Mn–N–C}$ : 157.95(11)° and 139.20(9)°) [28],  $[\text{Cu}(\text{NCS})_2(\text{C}_6\text{H}_8\text{N}_2)_2]$  ( $\angle\text{Cu–N–C}$ : 127.49(10)°) [29] and  $[\text{Cu}(\text{bedmpza})(\text{NCS})_2]$  ( $\angle\text{Cu–N–C}$ : 140.75(10)° and 173.44(11)°) [30].

### 3.7. $[\text{Mn}(\text{NO}_3)(\text{dca})(\text{tppz})]_n$ (**8**)

The structure **8** consists of neutral  $[\text{Mn}(\text{NO}_3)(\text{dca})(\text{tppz})]$  molecules linked by a single *end-to-end* dicyanamido group to an infinite one-dimensional zig-zag chain propagated along the [010] direction (Fig. 3).

The dicyanamido ligand is angular with a C(99)–N(97)–C(98) angle of 126.8(3)° and two nearly linear N–C–N units with angle of 170.3(3)°. The intrachain Mn···Mn separation of 8.784 Å falls in the range reported for the Mn(II) coordination polymers based on  $\mu_{1,5}$ -N(CN)<sub>2</sub> bridges, e.g.  $\{[\text{Mn}(\text{azpy})_2(\text{dca})(\text{H}_2\text{O})_2]-(\text{ClO}_4)(-\text{azpy})(\text{H}_2\text{O})_2\}_n$  (8.425 Å) [31a]  $\text{Mn}[\text{N}(\text{CN})_2]_2(\text{H}_2\text{O})_2(2,5\text{-me}_2\text{pyz})_2$  (8.425 Å) [31b]. Each manganese center is seven-coordinated by three N atoms from the *tppz* ligand, two oxygen atoms of the nitrate ligand and two nitrogen atoms belonging to  $\mu_{1,5}$ -bridged *dca*. The coordination polyhedron of Mn(II) ions is best described as pentagonal bipyramid with the equatorial plane being defined by nitrogen atoms of *tppz* and nitrate oxygen donors. Similarly to the mononuclear complexes (**5** and **6**), the nitrate group coordinates in a symmetric bidentate mode to the central ion (Table S8). The *tppz* ligand is significantly twisted. The pyrazine ring is puckered with maximum atomic deviations from a best mean plane being 0.0644(15) Å at C(4), and the dihedral angles between the pyrazine ring and each of the pyridyl rings are equal 27.00(9)°, 25.83(10)°, 44.64(11)° and 73.76(6)°. The coordination bond lengths and angles, reported in Table S10, are not unexceptional and correlate well with the values discussed for structures **1–7** and given for the related complexes  $[\text{Mn}(\text{NO}_3)(\text{dca})(\text{tppz})(\text{H}_2\text{O})_2]$

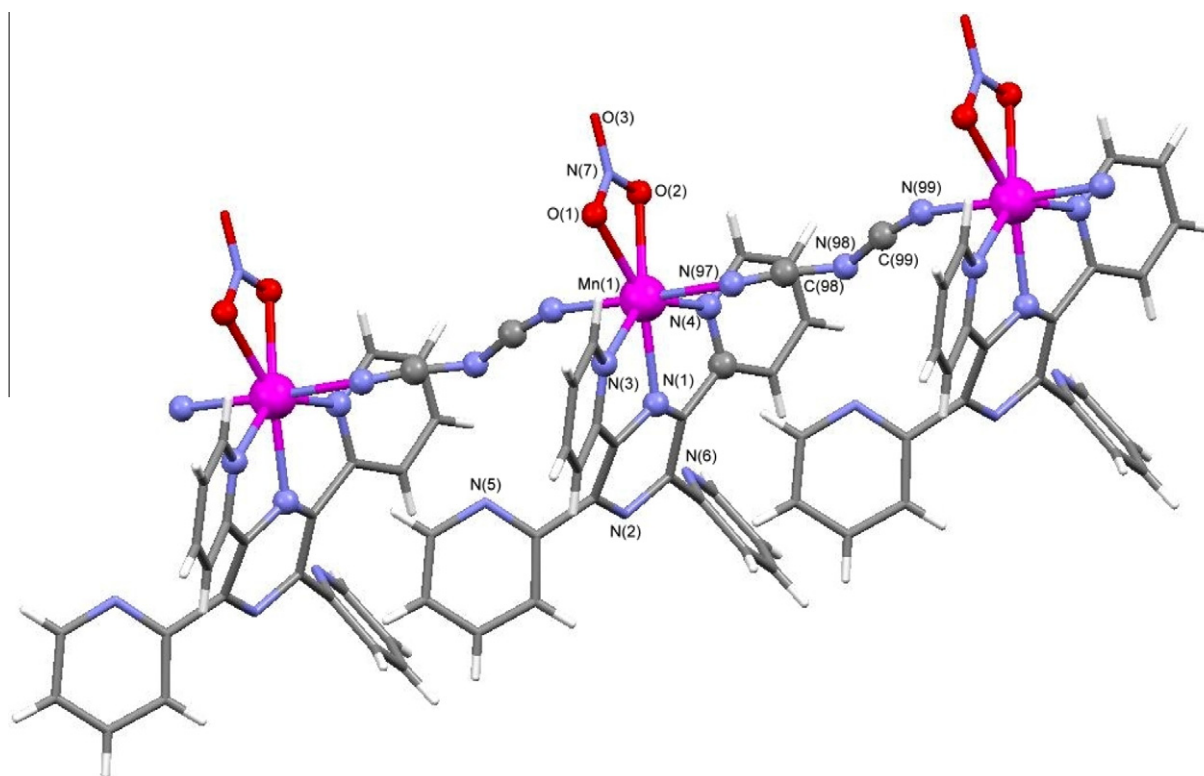


Fig. 3. The one-dimensional coordination chain of **8**.

O)] [32a], [Mn(CH<sub>3</sub>COO)(dca)(tppz)(H<sub>2</sub>O)]·(H<sub>2</sub>O)<sub>2</sub> [32b] and [Mn(dca)(NO<sub>3</sub>)(terpy)]<sub>n</sub> [32c].

### 3.8. Continuous shape measures (CShM)

The distortion of the coordination sphere of the Mn(II) ions in **1–8** from ideal polyhedra has been calculated using the SHAPE program [33] based on continuous shape measures (CShM) concept. CShM allows to determine a distance between the real metal environment and ideal polyhedron. Mathematically CShM of the original structure (*Q*) is a normalized root-mean-square deviation from the referenced structure with the desired symmetry (*P*) and it is expressed by Eq. (1):

$$S_Q(P) = \min \left[ \frac{\sum_{i=1}^n |\vec{q}_i - \vec{p}_i|^2}{\sum_{i=1}^n |\vec{q}_i - \vec{q}_0|^2} \right] \times 100 \quad (1)$$

where,  $\vec{q}_i$  are *N* vectors that contain the 3*N* Cartesian coordinates of the problem structure *Q*, and  $\vec{p}_i$  contain the coordinates of the ideal polyhedron *P* and  $\vec{q}_i$  is the position vector of the geometric center that is chosen to be the same for the two polyhedra [33,34]. The minimum is taken for all possible relative orientations in space, isotropic scaling, and for all possible pairings of the vertexes of the problem and reference polyhedra. The value  $S_Q(P)$  tends to zero, when considered polyhedron *Q* is close to ideal one [21g]. The maximum allowed value  $S_Q(P)$  is 100, although in practice the values found for severely distorted chemical structures are very rarely larger than 40.

The results of shape measurements for Mn(II) ions in the examined structures are summarized in Table S11.

Metal centers of compounds **1–4** present a six-coordinated environment and their geometries were referred to two ideal polyhedra: octahedron (O<sub>h</sub>) and trigonal prism (TPR). The most characteristic distortion of these systems is the Bailar trigonal twist, which leading from perfect octahedron to perfect trigonal prism and results from rotating by 60° two opposite faces of the octahedron around their C<sub>3</sub> axis [35]. In case when only two ideal polyhedra are taken into consideration (as for **1–4** octahedron and trigonal prism), each distortion can be represented by specific scatterplot in two-dimensional space defined by the two symmetry measures  $S_Q(O_h)$  and  $S_Q(TRP)$ . This scatterplot is called a shape map [34]. Fig. S6 shows the octahedron–trigonal pathway and includes the calculated shape measures for coordination sphere of the experimental structures **1–4**. For all compounds **1–4**,  $S(O_h)$  is lower than value 4.42 corresponding to the intermediate geometry (with  $\theta = 30^\circ$ ) being isosymmetric with respect to the octahedron and the trigonal prism. Therefore, the structures **1–4** are closer to an octahedron than to a trigonal prism and can be best described as a distorted octahedron. Dimers **1** and **2** are more distorted in comparison with mononuclear complexes **3** and **4**, and azide

bridges cause a larger distortion than chloride ions. In turn, analysis of Fig. 9 reveals that calculated shape measures for coordination sphere of the structures **1–4** do not appear along the Bailar path. Such deviation is typical for six-coordinated complexes incorporating polydentate ligands with small bite angles.

Manganese(II) ions of the complexes **5**, **6** and **8** are seven-coordinated and their geometries were referred to three commonly seven-vertexes polyhedra: pentagonal bipyramid (PBPY), capped octahedron (COC) and capped trigonal prism (CTP). The CShM of manganese(II) ions in compounds **5**, **6** and **7** revealed that their geometry is closer to pentagonal bipyramid (PBPY) than to the other seven-vertexes polyhedron (Table S11). The distances to the capped octahedron (COC) and capped trigonal prism (CTP) are much larger than to the PBPY. Generally, it is assumed that shape measures of less than 1.0 indicate minor distortions from the reference shape values of up to 3.0 units indicate important distortions, but the reference shape provides still a good stereochemical description.

Two ideal shapes, the trigonal bipyramid (TBP) of *D*<sub>3h</sub> symmetry, and the square pyramid (SPY) of *C*<sub>4v</sub> symmetry, were taken into account in continuous shape measures for geometry of the pentacoordinated metal center in **7**. The CShM values (Table S11) indicate the predominance of square-based pyramidal (SP) geometry of the manganese(II) ion in structure **7** and well correlate with the value of angular parameter  $\tau = 0.36$  also describing the structure **7** as a distorted square pyramid [36].

### 3.9. Magnetic properties and EPR spectra

The values  $\chi_M T$  of monometallic complexes in the temperature range 10–300 K are near constant. The slight decrease of the value  $\chi_M T$  at the lowest temperatures range (1.8–10 K) is caused by occurrence of a very weak antiferromagnetic interactions between Mn(II) centers in the crystal lattice. All magnetic data are presented in Table 3.

The variation of the magnetization *M* versus the magnetic field *H* have been measured for all complexes at 2 K indicates linear relation to ~1 T and than continues Brillouin function. All these data confirms presence of spin  $S = 5/2$  and a small lowering values of magnetic moment of manganese(II) centers. The EPR parameters of powdered spectra of all compounds are presented in the Table S12.

For monometallic complexes the magnetic data were fitted using the susceptibility equation for  $S = 5/2$  (Eq. (2)). To elucidate the significance of exchange between manganese(II) ions in the crystal lattices, a molecular field correction term [37] was also included (Eq. (3)).

$$\chi_M = \frac{N\beta^2 g^2}{3kT} S(S+1) \quad (2)$$

**Table 3**  
Magnetic parameters and magnetization data for complexes **1–8**.

Compound	$\chi_{dia}^a \times 10^6$ (cm <sup>3</sup> mol <sup>-1</sup> )	Curie constant <sup>b</sup> <i>C</i> (cm <sup>3</sup> K mol <sup>-1</sup> )	Weiss constant <sup>b</sup> $\theta$ (K)	Effective magnetic moments $\mu_B$ (B.M.)		Magnetization <sup>c</sup> (B.M.)
				<i>T</i> = 1.8 K	<i>T</i> = 300 K	
[Mn <sub>2</sub> (μ-Cl) <sub>2</sub> Cl <sub>2</sub> (tppz) <sub>2</sub> ] ( <b>1</b> )	-290	4.21	0.0	5.65	5.77	4.47
[Mn <sub>2</sub> Cl <sub>2</sub> (μ <sub>1,1</sub> -N <sub>3</sub> ) <sub>2</sub> (tppz) <sub>2</sub> ] ( <b>2</b> )	-391	4.10	-0.4	4.92	5.63	4.73
[MnCl(SCN)(tppz)(H <sub>2</sub> O)]·H <sub>2</sub> O ( <b>3</b> )	-273	4.35	-1.1	4.74	5.95	4.52
[Mn(NO <sub>3</sub> ) <sub>2</sub> (tppz)(H <sub>2</sub> O)] ( <b>5</b> )	-286	4.34	-0.22	5.52	5.85	4.88
[Mn(N <sub>3</sub> )(NO <sub>3</sub> ) <sub>2</sub> (tppz)(H <sub>2</sub> O)] ( <b>6</b> )	-219	3.94	-2.8	3.21	5.48	4.74
[Mn(SCN) <sub>2</sub> (tppz)] ( <b>7</b> )	-303	4.28	-1.9	3.51	4.70	4.31
[Mn(NO <sub>3</sub> )(dca)(tppz)] <sub>n</sub> ( <b>8</b> )	-251	4.33	-2.5	3.66	5.81	4.72

<sup>a</sup> Diamagnetic corrections calculated per one manganese center.

<sup>b</sup> In the temperature range 1.8–300 K.

<sup>c</sup> At the magnetic field 5 T and temperature 2 K.

**Table 4**  
Magnetic parameters<sup>a</sup> for complexes 1–7.

Compound	Exchange parameter $J$ (cm <sup>-1</sup> )	Intermolecular interaction $zJ'$ (cm <sup>-1</sup> )	Tensor $g$	Agreement factor $R$
[Mn <sub>2</sub> (μ-Cl) <sub>2</sub> Cl <sub>2</sub> (tppz) <sub>2</sub> ] ( <b>1</b> )	0.15	-0.08	1.95	6.11 × 10 <sup>-5</sup>
[Mn <sub>2</sub> Cl <sub>2</sub> (μ <sub>1,1</sub> -N <sub>3</sub> ) <sub>2</sub> (tppz) <sub>2</sub> ] ( <b>2</b> )	0.32	-0.16	1.91	6.00 × 10 <sup>-4</sup>
[MnCl(SCN)(tppz)(H <sub>2</sub> O)]·H <sub>2</sub> O ( <b>3</b> )		-0.13	1.99	6.68 × 10 <sup>-4</sup>
[Mn(NO <sub>3</sub> ) <sub>2</sub> (tppz)(H <sub>2</sub> O)] ( <b>5</b> )		-0.03	1.99	2.03 × 10 <sup>-4</sup>
[Mn(N <sub>3</sub> )(NO <sub>3</sub> ) <sub>2</sub> (tppz)(H <sub>2</sub> O)] ( <b>6</b> )		-0.88	1.94	2.75 × 10 <sup>-3</sup>
[Mn(SCN) <sub>2</sub> (tppz)] ( <b>7</b> )		-0.22	1.98	1.37 × 10 <sup>-3</sup>

<sup>a</sup> Calculated for the temperature range 1.8–300 K.

$$\chi_M^{corr} = \frac{\chi_M}{1 - \frac{2zJ'}{N\beta^2 g^2} \cdot \chi_M} \quad (3)$$

where  $N$  is the Avogadro's number,  $g$  is the tensor,  $\beta$  is the Bohr magneton,  $k$  is the Boltzmann constant,  $zJ'$  is the intermolecular exchange parameter and  $z$  is the number of the nearest neighbors of Mn(II) center.

The least-squares fit of the experimental data using these equations were limited to the temperature range from 1.8 K up to 300 K (Table 4).

The magnetic data of 1D chain complex indicated weak antiferromagnetic properties and have been fit using Fisher's classical Heisenberg results [38] for infinite linear chains.

The molecular field approximation has been used to account for interaction between chains. Fisher's Eq. (4) for magnetic susceptibility of a classical spin chain is:

$$\chi = \frac{Ng^2 \beta^2 S(S+1)}{3kT} \frac{1+u}{1-u} \quad (4)$$

with

$$u = \coth \left[ \frac{JS(S+1)}{kT} \right] - \left[ \frac{kT}{JS(S+1)} \right]$$

where  $J$  is the intrachain exchange parameter. If there are interaction between chains, the actual observed susceptibility may then be obtained using results of a molecular field calculation (Eq.

(3)), where  $J'$  is the interaction between chains and  $z$  is the number of nearest neighbor chains.

The least-squares fit of the experimental data using this equation was limited to the whole temperature range from 1.8 K up to 300 K and leads to  $J = -0.1$  cm<sup>-1</sup>,  $zJ' = -0.0$  cm<sup>-1</sup> and  $g = 1.97$  with the agreement factor  $R$  equal  $6.9 \times 10^{-5}$  for complex **8**. Experimental magnetic data plotted as  $\chi_M T$  versus  $T$  for 1D chain complex are shown in Fig. S7.

Weak ferromagnetic behaviours of dinuclear compounds are evident from the magnetic measurements. The  $\chi_M T$  value increases only at the lowest temperature, reaching maximums at 3.3 K and 16 K and then decreases on cooling down to 1.8 K. for **1** and **2** compound, adequate.

The magnetic data for dinuclear complexes were fitted using the susceptibility equation for Mn(II) center with  $S = 5/2$  and expressed by Eq. (5) [39].

$$\chi = \frac{N\beta^2 g^2}{kT} \frac{55 + 30e^{5x} + 14e^{9x} + 5e^{12x} + e^{14x}}{11 + 9e^{5x} + 5e^{9x} + 7e^{9x} + 5e^{12x} + 3e^{14x} + e^{15x}} \quad (5)$$

where  $x = -2J/kT$  and  $J$  is intradimer exchange interaction parameter.

To elucidate the significance of exchange between manganese(II) ions in the crystal lattices, a molecular field correction term [33] was also included, (Eq. (3)).

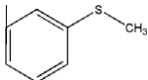
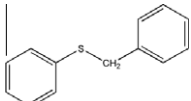
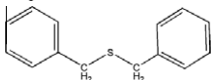
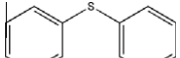
Experimental magnetic data plotted as  $\chi_M T$  versus  $T$  for complex **1** are shown in Fig. S8.

**Table 5**  
Oxidation of alcohols by the catalyst Oxone/*n*-Bu<sub>4</sub>NBr catalytic system.<sup>a</sup>

Entry	Substrate	Product	GC yield%	
			Compound <b>5</b>	Compound <b>6</b>
1			100	100
2			100	100
3			100	100
4			100	100
5			100	100
6			92	93
7			93	93
8			94	91

<sup>a</sup> The molar ratios for catalyst:phase transfer agent:substrate:oxidant are 1:10:20:20, respectively. The reactions were run for 5 min at room temperature in a biphasic medium (CH<sub>2</sub>Cl<sub>2</sub>/H<sub>2</sub>O).

**Table 6**  
Oxidation of sulfides catalyzed by **5** and **6**.<sup>a</sup>

Entry	Substrate	GC yield % <sup>b</sup>		Selectivity to sulfoxide (%) <sup>c</sup>
		Compound <b>5</b>	Compound <b>6</b>	
1		45	46	100
2		53	49	100
3		59	57	100
4		44	47	100
5	CH <sub>3</sub> CH <sub>2</sub> -S-CH <sub>2</sub> CH <sub>3</sub>	33	39	100

<sup>a</sup> The molar ratios for catalyst:imidazole:substrate:UHP are 1:10:20:40. The reactions were performed in (1:1) mixture of CH<sub>2</sub>Cl<sub>2</sub>/CH<sub>3</sub>OH (1 mL) under air at room temperature.

<sup>b</sup> The GC yield (%) are measured relative to the starting sulfide after 60 min.

<sup>c</sup> Selectivity to sulfoxide = (sulfoxide%/(sulfoxide% + sulfone%)) × 100.

The least-squares fit of the experimental data for both ferromagnetic complexes are presented in Table 4.

For all equations, the criterion used in determination of the best fit was based on minimization of the sum of squares of the deviation:

$$R = \sqrt{\frac{\sum_{i=1}^n \frac{1}{(\chi_i^{\text{exp}})^2} (\chi_i^{\text{exp}} - \chi_i^{\text{calc}})^2}{\sum_{i=1}^n \frac{1}{(\chi_i^{\text{exp}})^2}}}$$

### 3.10. Catalytic experiments

In order to compare catalytic reactivity of **5** and **6** with other compounds, we used the same optimization condition with our previous work [15a,b]. Reactions were performed at room temperature under air in CH<sub>2</sub>Cl<sub>2</sub>/H<sub>2</sub>O containing the manganese complex, tetra-*n*-butylammonium bromide, substrate and Oxone in 1:20:10:20 molar ratio, respectively. The system was applicable for the oxidation of a wide variety of primary benzylic alcohols to corresponding aldehydes (Table 5).

Benzylalcohols were oxidized to give the corresponding aldehydes with 91–100% conversion (entries 1–8). The substrates having electron-donating and -withdrawing substituents in the aromatic ring were compatible with this protocol. The change of nature and site of substituents (methyl, methoxy, chloro and nitro) in the aromatic ring of benzylalcohol to probe electronic effects displayed no regular trends in the conversion. The catalytic oxidation of alcohols in the given conditions showed excellent efficiency in terms of yield and selectivity (100%).

Also various types of structurally diverse substrates underwent smooth and selective oxidation to produce the corresponding sulfioxides in good yields. In order to compare catalytic reactivity of **5** and **6** with other Mn(II) complexes, we used the same optimization condition with our previous work [15c]. Aliphatic and aromatic sulfides were effectively oxidized to the corresponding sulfoxides with full selectivity and no over oxidation to sulfone were observed (Table 6).

Generally, the result of catalytic studies using these two catalysts reveals that the efficiency of catalysts **5** and **6** towards all the substrates is almost the same in term of conversion and selectivity. The complexes show prolific catalytic activity in the oxidation of various sulfides and alcohols.

## 4. Conclusions

Several novel halide and pseudohalides manganese(II) complexes containing *tppz* ligand have been synthesized and fully characterized. The studies have shown that the choice of manganese(II) salt is crucial in the formation of manganese(II) complexes with *tppz* and pseudohalide ligands. In the reported compounds the manganese(II) ions show various coordination geometries but *tppz* ligand coordinates to metal center in the most common tridentate coordination mode. Manganese(II) ions of 1D chain network [Mn(NO<sub>3</sub>)(dca)(*tppz*)]<sub>n</sub> are linked by a single *end-to-end* dicyanamido group, whereas the metal center of dimers [Mn<sub>2</sub>(μ-Cl)<sub>2</sub>Cl<sub>2</sub>(*tppz*)<sub>2</sub>] and [Mn<sub>2</sub>Cl<sub>2</sub>(μ-N<sub>3</sub>-κN1)<sub>2</sub>(*tppz*)<sub>2</sub>] are bridged by chloride and azide ions, respectively. Future studies will be focused on design of *tppz*-bridged manganese(II) complexes.

## Acknowledgements

This research was supported by the National Science Centre (Poland) under grant No. 2011/01/B/ST5/01624. M.M.N. is grateful to the Institute for Advanced Studies in Basic Sciences for financial support.

## Appendix A. Supplementary data

CCDC 896713, 896714, 896715, 896716, 896717, 896718, 896719 and 896720 contain the supplementary crystallographic data for C<sub>48</sub>H<sub>32</sub>Cl<sub>4</sub>Mn<sub>2</sub>N<sub>12</sub> (**1**), C<sub>48</sub>H<sub>32</sub>Cl<sub>2</sub>Mn<sub>2</sub>N<sub>18</sub> (**2**), C<sub>25</sub>H<sub>20</sub>ClMnN<sub>7</sub>O<sub>2</sub>S (**3**), C<sub>26.47</sub>H<sub>18.94</sub>ClMnN<sub>9</sub>O (**4**), C<sub>24</sub>H<sub>18</sub>MnN<sub>8</sub>O<sub>7</sub> (**5**), C<sub>24</sub>H<sub>18</sub>MnN<sub>10</sub>O<sub>4</sub> (**6**), C<sub>26</sub>H<sub>16</sub>MnN<sub>8</sub>S<sub>2</sub> (**7**) and C<sub>26</sub>H<sub>16</sub>MnN<sub>10</sub>O<sub>3</sub> (**8**). These data can be obtained free of charge via <http://www.ccdc.cam.ac.uk/conts/retrieving.html>, or from the Cambridge Crystallographic Data Centre, 12 Union Road, Cambridge CB2 1EZ, UK; fax: +44 1223-336-033; or e-mail: deposit@ccdc.cam.ac.uk. Supplementary data associated with this article can be found, in the online version, at <http://dx.doi.org/10.1016/j.poly.2013.01.015>.

## References

- [1] H.A. Goodwin, F. Lions, *J. Am. Chem. Soc.* 81 (1959) 6415.
- [2] (a) C.W. Padgett, W.T. Pennington, T.W. Hanks, *Cryst. Growth Des.* 5 (2005) 737;  
(b) M. Trivedi, D.S. Pandey, N.P. Rath, *Inorg. Chim. Acta* 362 (2009) 284;  
(c) L.M. Callejo, G. Madariaga, L. Lezama, L. Fidalgo, N. De la Pinta, R. Cortés,

- Inorg. Chem. 49 (2010) 5353;  
 (d) M. Maekawa, T. Minematsu, H. Konaka, K. Sugimoto, T. Kuroda-Sowa, Y. Suenaga, M. Munakata, Inorg. Chim. Acta 357 (2004) 3456.
- [3] (a) J. Yuasa, S. Fukuzumi, J. Am. Chem. Soc. 128 (2006) 15976;  
 (b) J. Yuasa, S. Fukuzumi, J. Am. Chem. Soc. 130 (2008) 566.
- [4] J. Carranza, C. Brennan, J. Sletten, J.M. Clemente-Juan, F. Lloret, M. Julve, Inorg. Chem. 42 (2003) 8716.
- [5] M. Graf, H. Stoeckli-Evans, A. Escuer, R. Vicente, Inorg. Chim. Acta 257 (1997) 89.
- [6] J. Carranza, J. Sletten, C. Brennan, F. Lloret, J. Cano, M. Julve, Dalton Trans. (2004) 3997.
- [7] (a) H.W. Richardson, W.E. Hatfield, J. Am. Chem. Soc. 98 (1976) 835;  
 (b) H.W. Richardson, J.R. Wasson, W.E. Hatfield, Inorg. Chem. 16 (1977) 484;  
 (c) J. Darriet, M.S. Haddad, E.N. Duesler, D.N. Hendrickson, Inorg. Chem. 18 (1979) 2679;  
 (d) M. Julve, M. Verdaguier, J. Faus, F. Tinti, J. Moratal, A. Monge, E. Gutiérrez-Puebla, Inorg. Chem. 26 (1987) 3520;  
 (e) J.A. Real, G. De Munno, M.C. Muñoz, M. Julve, Inorg. Chem. 30 (1991) 2701;  
 (f) T. Otieno, R.C. Thompson, Can. J. Chem. 73 (1995) 275;  
 (g) P.A. Goddard, J. Singleton, P. Sengupta, R.D. McDonald, T. Lancaster, S.J. Blundell, F.L. Pratt, S. Cox, N. Harrison, J.L. Manson, H.I. Southerland, J.A. Schlüter, New J. Phys. 10 (2008) 083025.
- [8] (a) C.M. Hartshorn, N. Daire, V. Tondreau, B. Loeb, T.J. Meyer, P.S. White, Inorg. Chem. 38 (1999) 3200;  
 (b) N. Chanda, N.H. Laye, S. Chakraborty, R.L. Paul, J.C. Jeffery, M.D. Ward, G.K.J. Lahiri, Chem. Soc., Dalton Trans. (2002) 3496;  
 (c) N. Chanda, B. Sarkar, J. Fiedler, W. Kaim, G.K. Lahiri, Dalton Trans. (2003) 3550;  
 (d) D.M. Datterlbaum, C.M. Hartshorn, T.J. Meyer, J. Am. Chem. Soc. 124 (2002) 4938;  
 (e) S.H. Wadman, R.W.A. Havenith, F. Hartl, M. Lutz, A.L. Spek, G.P.M. van Klink, G. van Koten, Inorg. Chem. 48 (2009) 5685.
- [9] L.M. Toma, D. Armentano, G. De Munno, J. Sletten, F. Lloret, M. Julve, Polyhedron 26 (2007) 5263.
- [10] H. Kwang, Z. Kristallogr. NCS 226 (2011) 59.
- [11] H. Kwang, Acta Crystallogr., Sect. E 67 (2011) m1333.
- [12] L. Callejo, N. De la Pinta, P. Vitoria, R. Cortés, Acta Crystallogr., Sect. E 65 (2009) m68.
- [13] (a) R.A. Sheldon, J.K. Kochi, Metal-Catalyzed Oxidations of Organic Compounds, Academic Press, New York, 1981;  
 (b) G. Cainelli, G. Cardillo, Chromium Oxidations in Organic Chemistry, Springer, Berlin, 1984;  
 (c) R. Maggi, S. Chitsaz, S. Loebbecke, C.G. Piscopo, G. Sartori, M. Schwarzer, Green Chem. 13 (2011) 1121;  
 (d) G. Centi, F. Cavani, F. Trifiro, Selective Oxidation by Heterogeneous Catalysis, Kluwer Academic Publishers, New York, 2001.
- [14] (a) M. Bagherzadeh, M. Amini, D.M. Boghaei, M.M. Najafpour, V. McKee, Appl. Organomet. Chem. 25 (2011) 559;  
 (b) R.A. Sheldon, I.W.C.E. Arends, A. Dijkstra, Catal. Today 57 (2000) 157;  
 (c) S.K. Karmee, L. Greiner, A. Kraynov, T.E. Müller, B. Niemeijer, W. Leitner, Chem. Commun. 46 (2010) 6705;  
 (d) P.L. Maux, G. Simonneaux, Chem. Commun. 47 (2011) 6957.
- [15] (a) M.M. Najafpour, M. Amini, M. Bagherzadeh, D.M. Boghaei, V. McKee, Transition Met. Chem. 35 (2010) 297;  
 (b) M.M. Najafpour, M. Holyńska, M. Amini, H. Kazemi, T. Lis, M. Bagherzadeh, Polyhedron 29 (2010) 2837;  
 (c) M.M. Najafpour, M. Holyńska, A.N. Shamkhali, M. Amini, S.H. Kazemi, S. Zaynalpoor, R. Mohamadi, M. Bagherzadeh, T. Lis, Polyhedron 34 (2012) 202.
- [16] CrysAlis RED, Version 1.171.35.11, Oxford Diffraction Ltd., 2011.
- [17] G.M. Sheldrick, Acta Crystallogr., Sect. A 64 (2008) 112.
- [18] E. König, Magnetic Properties of Coordination and Organometallic Transition Metal Compounds, Springer, Berlin, 1966.
- [19] K. Nakamoto, Infrared and Raman Spectra of Inorganic and Coordination Compounds, fourth ed., Wiley-Interscience, New York, 1986.
- [20] (a) G.A. Jeffrey, W. Saenger, Hydrogen Bonding in Biological Structures, Springer-Verlag, 1994;  
 (b) G.R. Desiraju, T. Steiner, The Weak Hydrogen Bond in Structural Chemistry and Biology, Oxford University Press, 1999.
- [21] (a) J.-Z. Wu, E. Bouwman, A.M. Mills, A.L. Spek, J. Reedijk, Inorg. Chim. Acta 357 (2004) 2694;  
 (b) A. Garoufisa, S. Kasselouria, S. Boyatzis, C.P. Raptoulou, Polyhedron 18 (1999) 1615;  
 (c) P. Tyagi, U.P. Singh, J. Coord. Chem. 62 (2009) 1613;  
 (d) C.-M. Liu, S. Gao, D.-Q. Zhang, Z.-L. Liu, D.-B. Zhu, Inorg. Chim. Acta 358 (2005) 834;  
 (e) R. Cortés, J.L. Pizarro, L. Lezama, M.I. Arriortua, T. Rojo, Inorg. Chem. 33 (1994) 2697;  
 (f) H.-Y. Wu, H.-Q. An, B.-L. Zhu, S.-R. Wang, S.-M. Zhang, S.-H. Wu, W.-P. Huang, Inorg. Chem. Commun. 10 (2007) 1132;  
 (g) T.K. Karmakar, B.K. Ghosh, A. Usman, H.-K. Fun, E. Rivière, T. Mallah, G. Aromí, S.K. Chandra, Inorg. Chem. 44 (2005) 2391.
- [22] I. Romero, M.-N. Collomb, A. Deronzier, A. Llobet, E. Perret, J. Pécaut, L. Le Pape, J.-M. Latour, Eur. J. Inorg. Chem. 40 (2001) 69.
- [23] R. Ahmadi, K. Kalateh, V. Amani, Acta Crystallogr., Sect. E 66 (2010) m959.
- [24] J. Kožisek, J. Marek, Z. Baloghová, D. Valigura, Acta Crystallogr., Sect. C 53 (1997) 1813.
- [25] O.V. Shishkin, K.Y. Pichugin, L. Gorb, J. Leszczyński, J. Mol. Struct. 616 (2002) 159.
- [26] G.J. Kleywegt, W.G.R. Wiesmeijer, G.J. Van Driel, W.L. Driessen, J. Reedijk, J.H. Noordik, J. Chem. Soc., Dalton Trans. (1985) 2177.
- [27] F.H. Allen, Acta Crystallogr., Sect. B 58 (2002) 380.
- [28] S. Sasi, M. Sithambaresan, M.R. Prathapachandra Kurup, H.-K. Fun, Polyhedron 29 (2010) 2643.
- [29] N.K. Karan, K.-T. Chan, H.M. Lee, Acta Crystallogr., Sect. E 65 (2009) m525.
- [30] S.S. Massoud, L.L. Quan, K. Gatterer, J.H. Albering, R.C. Fischer, F.A. Mautner, Polyhedron 31 (2012) 601.
- [31] (a) L.-N. Zhu, Y. Ou-Yanga, Z.-Q. Liua, D.-Z. Liaoa, Z.-H. Jianga, S.-P. Yana, P. Chenga, Z. Anorg. Allerg. Chem. 631 (2005) 1693;  
 (b) J.L. Manson, J.A. Schlüter, U. Geiser, M.B. Stone, D.H. Reich, Polyhedron 20 (2001) 1423.
- [32] (a) L. Callejo, N. De la Pinta, P. Vitoria, R. Cortés, Acta Crystallogr., Sect. E 65 (2009) m68;  
 (b) A. Majumder, G. Pilet, M.T.G. Rodriguez, S. Mitra, Polyhedron 25 (2006) 2550;  
 (c) A. Claramunt, A. Escuer, F.A. Mautner, N. Sanz, R. Vicente, J. Chem. Soc., Dalton Trans. (2000) 2627.
- [33] M. Llunell, D. Casanova, J. Cirera, M. Bofill, P. Alemany, S. Alvarez, M. Pinsky, D. Avnir, SHAPE program, version 1.1b, Barcelona, 2003.
- [34] (a) D. Casanova, J. Cirera, M. Llunell, P. Alemany, D. Avnir, S. Alvarez, J. Am. Chem. Soc. 126 (2006) 1755;  
 (b) E.M. Zueva, E.R. Ryabikh, S.A. Borshch, Inorg. Chem. 50 (2011) 11143.
- [35] S. Alvarez, D. Avnir, M. Llunell, M. Pinsky, New J. Chem. 26 (2002) 996.
- [36] A.W. Addison, T.N. Rao, J. Reedijk, J. Rijn, G.C. Verschoor, J. Chem. Soc., Dalton Trans. (1984) 1349.
- [37] J. Samuel, Smart, Effective Field Theories of Magnetism, W.B. Saunders Comp., Philadelphia and London, 1966.
- [38] M.E.E. Fisher, Am. J. Phys. 32 (1964) 343.
- [39] A. Earnshaw, J. Lewis, J. Chem. Soc. (1961) 396.